3D Quantitative Analysis of Platinum Nanocrystal Superlattices by Electron Tomography

Ileana Florea,[†] Arnaud Demortière,[‡,§] Christophe Petit,[‡] Hervé Bulou,[†] Charles Hirlimann,[†] and Ovidiu Ersen[†,*]

[†]Institut de Physique et Chimie des Matériaux de Strasbourg, UMR 7504, CNRS-UdS, 23 rue du Lss BP43, 67034 Strasbourg cedex 2, France, [‡]Laboratoire des Matériaux Mésoscopiques et Nanométriques, UMR 7070, CNRS-UPMC, 4 place Jussieu, 75252 Paris cedex 05, France, and [§]Center for Nanoscale Materials, Argonne National Laboratory, 9700 South Cass Avenue, Argonne, Illinois 60439, United States

ABSTRACT The work reported herein focuses on the 3D relative arrangement of individual platinum nanocrystals with a size of about 5 nm, and on the structure of the superlattices, they spontaneously form. Electron tomography was systematically used in this study because it allows obtaining quantitative 3D information in real space. Performing tomography in the bright-field TEM mode allowed investigating the short and long-range orderings of the nanoparticles packed as self-organized supercrystals. Systematic fcc pilings were observed with a mean lattice parameter measured to be 19.5 nm, the nature of the arrangement being controlled by the truncated octahedral morphology of platinum nanocrystals and the associated steric effects. A numerical 3D quantitative analysis of the ordering characteristics of the superlattice with a nanometer resolution has been performed that, for the first time, showed a direct correlation between single entities' characteristics and their ordering in periodic arrays. It has been shown that the lattice parameter is different in two orthogonal directions of the fcc structure, which indicates the presence of a slightly compressed superlattice. Inside the superstructure, vacancies and axial defects were observed that would blur the occurrence of potential collective effects from the supercrystals.

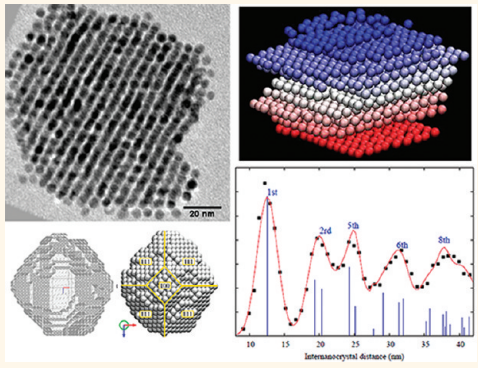

KEYWORDS: platinum nanocrystals · nanocrystal superlattices · 3D stacking · long-range order · electron tomography · pair distribution function

The assembly of nanocrystals into 3D ordered superstructures with a lattice parameter on the order of tens of nanometers has attracted increasing attention due to their potential to enhance a wide variety of applications based on collective optical[1] or magnetic[2] effects. Nanocrystal superlattices are a new type of artificial materials having properties that are controlled by the individual building blocks and also by their collective interactions. The assembly of nanocrystals (NCs) into ordered structure leads to the observation of unexpected physical behaviors, such as coherent vibrations that have been observed using Raman spectroscopy[3] and femtosecond laser pulses in a frequency range much smaller than in atomic or molecular crystals.[4] Another famous illustration of such collective effects is the electromagnetic energy transport in metal self-organized nanoparticle plasmon waveguides.[5−7] In this context, the recent advances in both the synthesis of colloidal nanocrystals[8] and the design of superstructures[9] have opened up great opportunities for fundamental investigations of structural and physical properties of superlattices. From the viewpoint of the structural study of these nanodevices, it becomes necessary to analyze the arrangement of crystals into packing on more local bases. The packing symmetries and densities strongly depend on the shape of the NCs and on their relative positions. In particular, a large long-range ordered superlattice requires a narrow size distribution of a unique shape. Therefore, these parameters must be precisely controlled before the ordering of the particles, preferentially at the time of the synthesis. The existence of minor facets on the NCs can lead to other packing symmetries, such as body-centered cubic (bcc)[10] or nematic liquid-crystal-like phases.[11]

This work reports on the 3D characterization of self-ordered platinum NC superlattices. One of the major challenges here was to carry out characterizations at both the scale of the nanoparticles and the scale of the lattice they form. For this purpose, techniques based on the Fourier analysis of the information obtained from X-rays and

* Address correspondence to ovidiu.ersen@ipcms.u-strasbg.fr.

Received for review December 22, 2011 and accepted February 9, 2012.

Published online February 15, 2012
10.1021/nn205029s

electron diffractions are commonly used. The main drawbacks of these scattering methods or of the associated ones are their inability to provide spatially resolved information and the need of producing hypotheses on the nanoparticles' morphology for interpreting the data. In addition, the analysis of the defects in the long-range ordering is difficult since these scattering methods are strongly model-dependent. In this context, the electron tomography technique which gives access to real space information is thus a strongly relevant tool to overcome the above-mentioned difficulties. Applied with a subnanometer resolution on a field of view of several hundreds of nanometers, this characterization technique makes it possible to work out specific information at three dimensions, providing thus spatial selectivity in the nanometer range. It consists in the volume reconstruction of a 3D specimen by using a series of its 2D projections recorded in one of the TEM modes compatible with the tomographic approach. In the specific case of self-assembled superlattices, it can achieve ordering characterization by detecting and classifying individual 3D defects in the structure when the scattering methods only provide access to global averaged order parameters. In spite of its impressive potential for the 3D characterization of the nanostructures, its regular implementation in the field of materials science started only 15 years ago.[12−14] One of the reasons was the presence of the diffraction contrast in the traditional TEM images recorded on crystalline materials; this phase contrast does not satisfy the projection requirement for the tomography that stipulates the image intensity must be proportional only to the mass and thickness of the specimen. Nowadays, several electron tomographic modes exist that are initiated by the large variety of imaging modes which have been made available in electron microscopy. For instance, the energy-filtered (EFTEM) mode enables one to provide elemental maps with a resolution in the nanometer range,[15−19] and the scanning TEM (STEM) mode uses a very convergent probe to explore the sample in a raster pattern and to record 2D images one pixel after the other by collecting different signals.[20] This last mode can be combined with the EDS or EELS spectroscopies, but its most usual implementation in electron tomography is applied to the acquisition of a series of bright-field and annular dark-field images. This last mode is actually very appropriate for the 3D analysis of crystalline nanomaterials, especially when high collection angles are used (in the so-called HAADF mode), as in this case the contribution of the Bragg diffraction by crystalline structures is strongly reduced when the recorded signal is incoherent.[12,21] However, it is worth noticing that, in the case of weakly scattering crystalline materials or the case of very small crystallites, the BF-TEM mode can also provide reliable 3D information,[22] with the advantage of an easy to implement technique especially concerning the acquisition step of the tilt series.

In this study of superlattices made out of crystalline nanoparticles having a very small size, the deleterious effect of the residual diffraction contrast in the reconstructed volume obtained by traditional TEM tomography is low because (i) the contribution of the diffraction contrast to the TEM images becomes less important when the crystallite size decreases; (ii) for single crystals the artificial changes in image intensity due to the diffraction contrast only appears for specific angles, and thus their contribution to the final reconstruction is canceled by the averaging of information originating from the whole tilt series. Furthermore, related to the study of these 3D nanostructures by electron tomography, the traditional TEM mode has a dual advantage compared to BF or ADF STEM: (i) the rapidity of the acquisition process enables the recording of a high number of images within a large angular interval, reducing thus the contribution of the reconstructions artifacts; (ii) the thickness of the in-focus part of the sample is larger, allowing thus the observation of thicker areas of specimen under study, which is fundamental for the study of superlattices. For these reasons, this tomographic study was performed in the usual TEM mode. Finally, it is worth noting that the present work is focused principally on the analysis of the periodical arrangement of the NCs into the superlattice, and that the precise study of their individual morphologies will be reported in another work.

Since the implementation of electron tomography in materials' field, some studies of 3D arrangements of NCs into superlattices have been published. One of the first experiments reports on the use of the traditional bright-field TEM tomography to reveal the shape of larger PbSe nanoparticles and their relative stacking in 3D arrays.[23] The accurate determination of the lattice parameters and distortions has also been carried out into binary superlattices made of spherical particles with different sizes (PbSe/Au, PbSe/CdSe)[24] and also into a bcc packing supercrystal composed by octahedral Pt_3Ni NCs of 10 nm size.[25] More recently, a 3D electron tomography study has been performed on self-assembled octapod nanocrystals, revealing an uncommon tetragonal structure.[26] However, though few recent papers were devoted to finding a correlation between the shape of nanoparticles and their long-range arrangement in ordered arrays,[27−29] no published work has reported up to now a numerical 3D quantitative analysis of the ordering characteristics of the NC superlattices.

In this context, we report here a 3D analysis of the relative arrangement of Pt NCs and their periodical stacking into 3D superlattices. For this purpose, a quantitative analysis of the reconstructed volumes obtained by using electron tomography is required, which permits the measurement of the parameters of

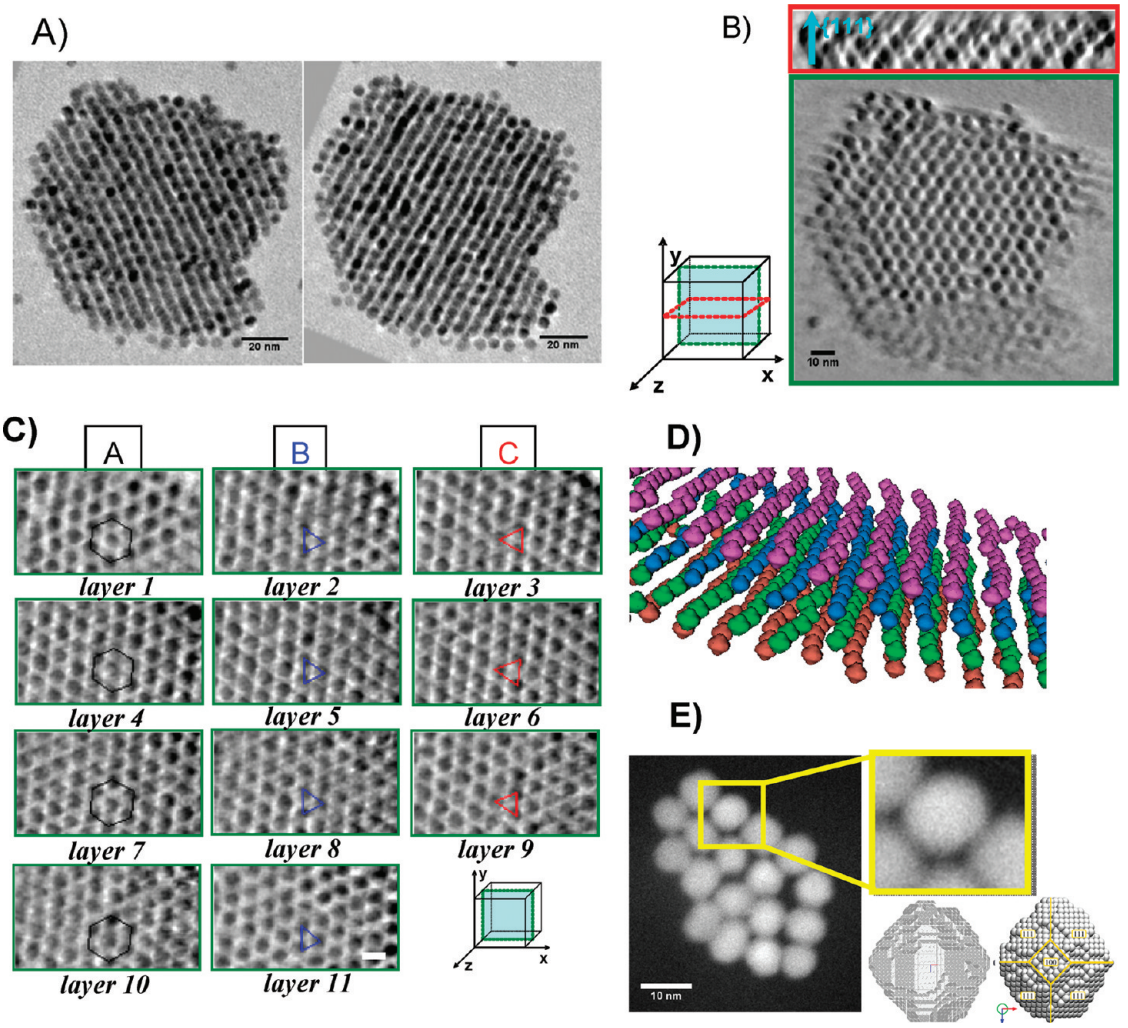

Figure 1. (A) Examples of BF-TEM images from the tilt series used to reconstruct the volume of a fragment of a meta-crystal, corresponding to 0 and 45° tilt angles. (B) Typical transverse and longitudinal slices through the reconstruction, showing the relative packing of the layers and the in-plane hexagonal symmetry. (C) Successive slices, separated by the mean distance between two monolayers of Pt NCs, through the reconstructed volume; any stacking fault is observed in the 3D stacking of NCs for the analyzed fragment; the 3D assembly contains 11 layers when looking along the direction corresponding to a six-fold symmetry axis in the packing of the Pt NCs. (D) Modeling of the first four layers of the studied assembly which contains 11 successive layers; the successive layers are depicted with different colors. (E) Synopsis of our separate work which has shown that the shape of individual Pt nanoparticles corresponds to a truncated octahedron.

the periodic array and the establishment of a relationship between the morphology previously deduced and the long-range ordering. Furthermore, the type and the density of the existing defects were also investigated from the reconstructed volumes of an assembly of NCs. Last, information on the spatial extension of the long-range ordering in the superlattice was obtained using a direct distance measure between NCs in the real space (PDF analysis).

RESULTS AND DISCUSSION

One of the main parameters governing the potential use in applications of these NC superlattices is the long-range order degree, in other words the spatial extension of the periodic arrangement of the NCs. In this context, the aim of the present analysis is to obtain reliable information on the 3D organization in the Pt supercrystals. For this purpose, several tomographic analyses were performed on representative fragments containing NC multilayers of NCs. The parameters of interest, which can be extracted from the 3D reconstruction, are the spatial positions of all of the NCs and also their individual mean size compared to an average value representing the whole assembly. In particular, the precise knowledge of the relative positions of the NCs allows, first, determining typical parameter characteristics of the long-range order, such as the superlattice parameter and the coherence length, and, second, to provide direct evidence on the point defects or the stacking defects. As explained in the introduction, to obtain reliable information, such an analysis must be performed on relatively large clusters, and consequently, the acquisitions were performed at mean magnification in BF-TEM mode.

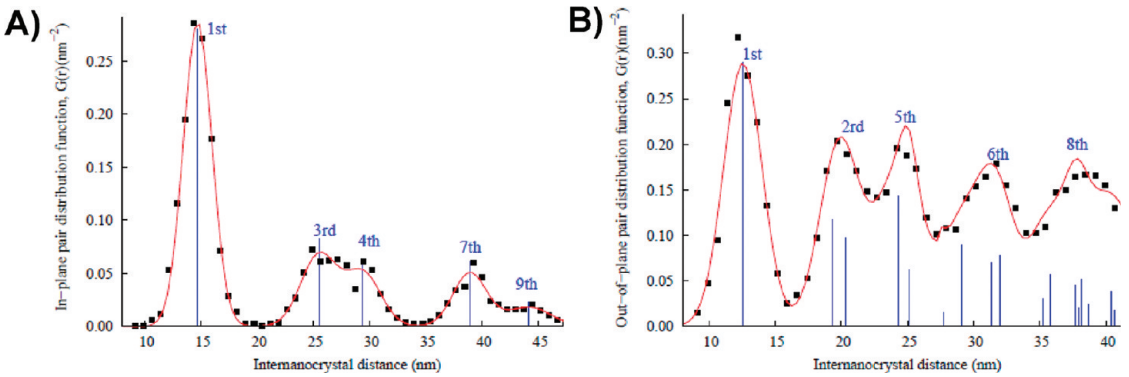

Figure 2. In-plane (A) and out-of-plane (B) pair distribution functions (PDF). The black square symbols represent the experimental PDFs, the blue lines represent the PDFs for a slightly distorted fcc structure, and the red lines represent the corresponding PDFs for disordered structures.

It is worth noting that information on the 3D periodical arrangement of NCs into a superlattice can also be deduced through electron diffraction experiments. However, the out-of-plane distances are much more difficult to obtain in the case of superlattices directly deposited on a TEM support membrane. In addition, the correlation length of 3D positions of NCs is rather limited in such superlattices, giving rise to broad diffraction spots and thus inaccurate values for distances; this is not the case for the artifact-free tomographic analysis, where the measurements are performed in the real space and are not limited to the study of highly ordered systems.

The necessary steps for performing the tomographic analysis are illustrated in Figure 1, where we present for one of the analyzed fragment some typical 2D TEM images (1A), then two numerical orthogonal sections crossing successive layers or parallel to the support (1B), and at last the modeling of the assembly where the various layers are depicted with various colors (1D). Furthermore, Figure 1C depicts several equidistant slices through the reconstructed volume, separated by the mean distance between two monolayers of Pt NCs oriented parallel to the support. By analyzing the stacking of these successive layers in this fragment that contains more than 10 layers, we systematically observed an ABC stacking alternation, characteristic of a face-centered cubic (fcc) structure. This suggests the absence of stacking faults in this superlattice, a typical defect often present in this type of arrangement. On the other hand, a simple inspection of the transverse sections shows that the spatial extension of single layers increases with the distance to the horizontal support, indicating that the presence of the substrate is not of prime importance for the 3D ordering process. As a general comment, thanks to its ability to give access to real space information, tomographic analysis provides useful information on the nucleation and growth mechanisms. Note that the limited 3D resolution in this reconstructed volume does not allow one to precisely solve the morphology of an individual nanoparticle located in the 3D stacking, which was rather the aim of another work.[30]

In order to precisely determine the relative 3D positions of the Pt NCs contained in the global reconstruction, the hard sphere model that assigns a spherical shape for each particle was used in a first approximation. A relevant parameter for characterizing the long-range order of the superlattices is the pair distribution function (PDF). It describes the density of interparticle distances in the superlattice. Figure 2 shows the associated in-plane and out-of-plane pair distribution functions (PDF). For the calculation, the two directions were separated in order to examine a potential effect due to different in-plane and out-of-plane superlattice parameters. A striking point evidenced from these figures is the large value of the long-range ordering. This good ordering inside the fragment is confirmed by the structure of the pair distribution functions (PDF) (Figure 2). In addition, a decrease of the intensity of the peaks when the intercluster distance increases is observed due to limited spatial extension of the superlattice. This intensity decrease is also governed by the broadening of the peak (inset in Figure 2B). Such a broadening is due to a limited coherence length of the NC positions. The first maximum, corresponding to the nearest neighbors (NN) distance between NCs, indicates an in-plane nearest neighbors distance of 14.65 $\pm$ 0.02 nm and an out-of-plane one of 12.93 $\pm$ 0.02 nm. The distance between two NCs is higher than their mean diameter, which confirms the presence of organic ligands (octylamine) on the platinum nanocrystal surfaces from their synthesis procedure. Four additional peaks are present in the in-plane PDF at 25.94 $\pm$ 0.01, 30.02 $\pm$ 0.20, 39.09 $\pm$ 0.19, and 44.28 $\pm$ 0.49 nm. They correspond, respectively, to the third, fourth, seventh, and ninth nearest neighbors. The absence of the second, fifth, sixth, and eighth nearest neighbors provides direct evidence of the presence of several monolayers with a six-fold symmetry perpendicular axis. A similar feature is observed for the out-of-plane PDF where the

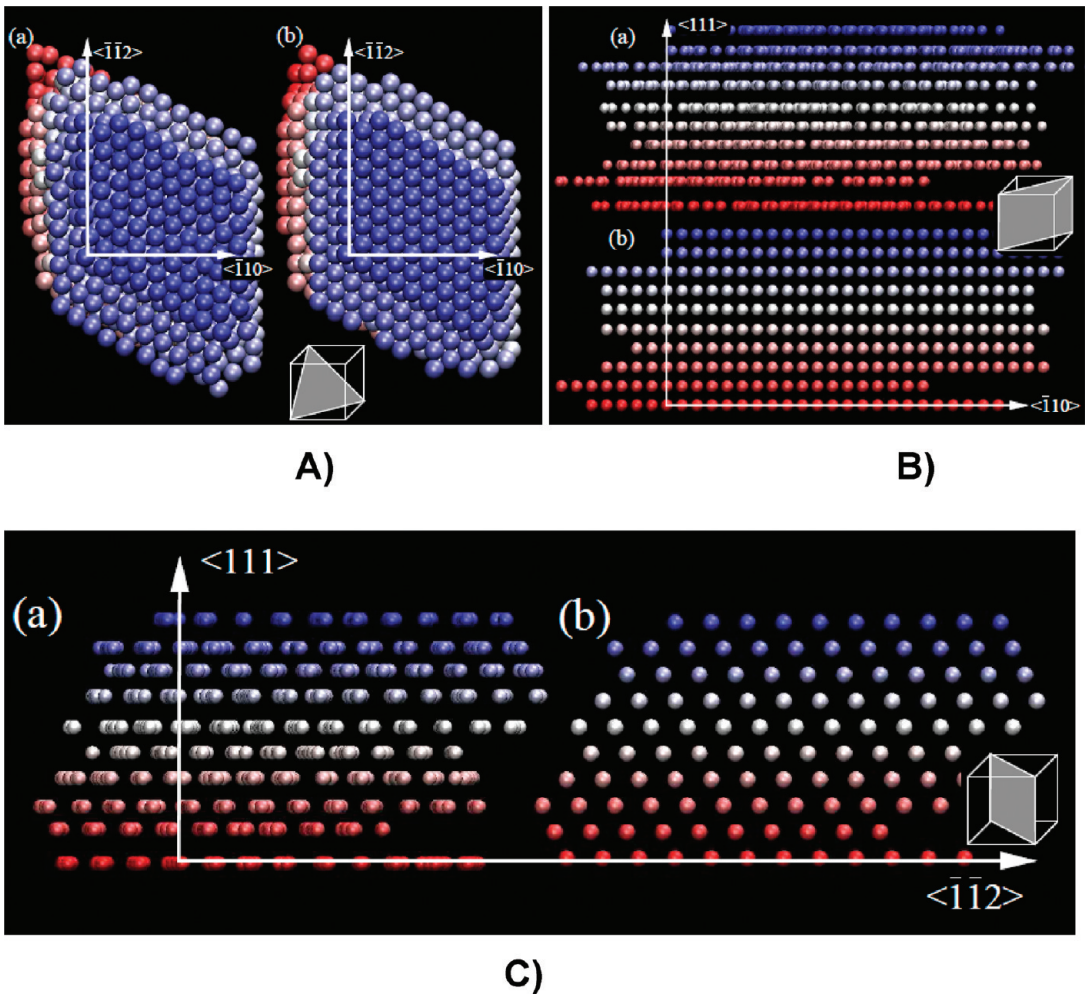

Figure 3. (A) Top view and (B,C) side views of (a) the experimental NCs assembly, (b) associated perfect superlattice, along three crystallographic axes. The experimental superlattice has been built from the 3D positions of the centers of NCs obtained by tomography, whereas the perfect ordered one has been constructed by considering the lattice in-plane and out-of-plane parameters deduced from the pair distribution functions of the experimental superlattice. For representation, we have considered spherical shapes for the NCs in both superlattices.

presence of peaks corresponding to the second, fifth, sixth, and eighth nearest neighbors strongly suggests the presence of a face-centered cubic structure. However, in such a structure, the significant difference between the in-plane and out-of-plane NN distances can be explained by the existence of two different lattice parameters of the cubic lattice in the two orthogonal directions, leading thus to a slight compression of the supercrystal lattice. An important remark at this stage of the analysis is that the difference between in-plane and out-of plane NN distances cannot be due to the elongation effect, generally present in the electron tomography reconstructions: on the one hand, with our acquisition parameters, the estimated value of the elongation factor is insignificant in first approximation (down to 1.1); on the other hand, this effect would induce an out-of-plane distance higher than the in-plane one, which is not the case here.

On the basis of the in-plane and out-of-plane parameters determined from the experimental PDF, we build up the corresponding theoretical distorted fcc structure. The associated PDFs are represented with blue lines in Figure 2; the positions and the intensities of the various peaks are in good agreement with those of the experimental PDFs, providing once again direct evidence of an fcc-type structure. A larger number of peaks are present in the out-of-plane PDF because of different in-plane and out-of-plane superlattice parameters. Additionally, the comparison between the experimental NC arrangement and the perfect one (Figure 3) evidences different degrees of ordering depending on the crystallographic direction. Note that the quantitative analysis of the NC arrangement in the 3D stacking does not necessitate the consideration of a perfect ordered lattice as an input, which was built only in order to allow a one-to-one comparison of the characteristics of two types of PDF peaks, in terms of height and width.

Once the morphology of a unique particle (of truncated octahedron type, as studied in our separate work[30])

and the periodical arrangement in a 3D array of an assembly of those are known, another parameter can be deduced from the 3D analysis as to say the relative orientation between the neighboring particles. Figure 4A presents the idealized 3D packing of a series of truncated octahedrons, as well as three corresponding orthogonal views, two side views (B and C) and the top view (D). A schematic representation of the in-plane packing is also represented (Figure 4F), with the {100} facets in blue and the {111} planes in red. Indeed, the relative packing of truncated octahedral nanoparticles organized in a hexagonal array is relatively well-known in the literature.[31] To check the relative orientation of Pt NCs in our superlattice, several 3D slices crossing the mass centers of some neighboring NCs have been extracted. A fragment from a typical slice is shown on Figure 4E. By inspecting these oriented slices, it appears that the NCs belonging to a 2D array have a spatial orientation similar to the idealized packing of truncated octahedrons, as represented in three dimensions on Figures 4A–D and in two dimensions on Figure 4F, imposed by the steric effect. As can be observed when looking at two orthogonal slices extracted from this 3D representation, the facets involved in the in-plane packing are the {111} and {100}, whereas in the out-of-plane directions, only the {111} facets play a role in the relative stacking of neighboring NCs. Such a difference in the contribution of the two facets to the in-plane and out-of-plane packing can explain the compression of the crystallographic lattice build by the 3D positions of the NPs. Additionally, the presence of two crystallographic facets involved in the in-plane packing can be at the origin of the existence of an anisotropic in-plane degree of ordering, as can be observed when comparing the side views of the 3D Pt NCs assembly represented on Figure 3B,C. As a final remark, it seems to be obvious that identical morphologies and relative orientations of the entities building up a superlattice are the main requirements to promote their periodical arrangement and both conditions seem to be realized in the present studied case.

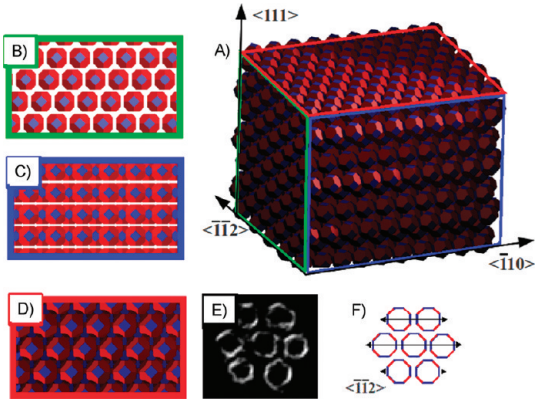

Figure 4. (A) Idealized representation of the 3D packing of truncated octahedron crystals organized in a hexagonal 2D array, as is the case of the monolayers contained in our superlattice. (B,C) Side views and (D) top view of the 3D supercrystal represented in (A). (E) Typical 2D slice extracted from the reconstructed volume showing the borders of several neighboring Pt NCs located in the same 2D hexagonal layer. (F) Two-dimensional schematic representation of a series of ideal truncated octahedrons organized in a hexagonal 2D layer, illustrating their in-plane packing. The {100} facets are represented in blue and the {111} in red.

The presence of defects in the periodical arrangement is another structural information that can be accessed using electron tomography. Once again, thanks to its ability to provide information directly in the real space, tomography allows detecting defects without the need for any modeling. In such systems, as in atomic crystals, the entropy governs the number and the types of organization defects. However, the kinetic effects that happen during the growth of the supercrystals can drastically increase this number of defects. Generally, their influence on the emerging properties of the superlattice strongly depends on the spatial extension and periodicity of the defects such as point or planar defects. Two types of organization defects were particularly observed in our superlattices. The first one is given by the presence of some individual vacancies localized in one of the successive layers (schematized by red circles in the longitudinal section presented in Figure 5A), without any real disturbance of the long-range organization for the neighboring NCs. A second type of defect that is observed by analyzing the reconstruction is an axial defect

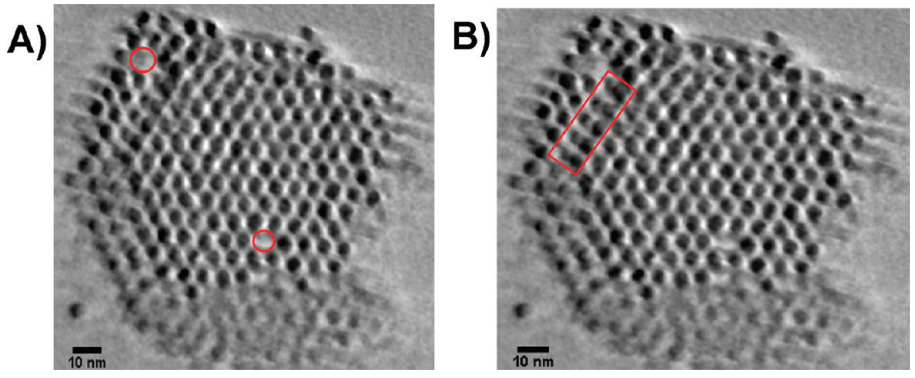

Figure 5. Two (111) slices revealing the presence of two individual vacancies in the superlattice (A) and of an axial defect (B).

(Figure 5B). One of the proposed hypotheses to explain its presence is the inhomogeneity of the organic ligand shell that is supposed to surround the NCs. From a general point of view, considerable work must be devoted to the adjustment of the synthesis conditions in order to drastically reduce the density of defects, as the supercrystal symmetry is broken at their location, inducing a blurring of the collective properties of the superlattice. As a general comment, it is worth noticing that quantifying defects by direct visualization or using automated routines seems to be an unavoidable extension for future studies in the field.

CONCLUSIONS

Using the ability of electron tomography to provide reliable 3D representations of objects in the real space, we reported here a complete structural study of Pt nanoparticle superlattices. The originality of this study is that it furnishes for the first time a relation between the joined morphology and long-range ordering, for really small nanoparticles having a complex morphology. The tomographic analysis directly provides the characteristics of the long-range order in the superlattices, without the need to compare the experimental data to simulations. As a separate study has demonstrated that the shape of Pt NCs is close to the truncated octahedron crystal, one can conclude here that the periodic arrangement of NCs on a fcc lattice originates mainly from the initial truncated octahedron morphology. We have shown here that the periodic arrangement of truncated octahedral NCs on such a fcc lattice presents an out-of-plan lattice compression that can be related to the influence of the $\{111\}$ facets in the relative stacking of neighboring NCs. Finally, the superlattice parameters were precisely determined and two different types of defects illustrated. Finally, a structure factor for the supercrystal was defined, which contains useful information on the spatial extension of the long-range ordering. Our findings underline once again the benefit and the uniqueness of this kind of multiscale analysis for the characterization of the self-assembled systems, where the individual morphology of the constitutive entities govern their periodic arrangement.

MATERIALS AND METHODS

Elaboration of Nanocrystal Superlattices. Pt nanocrystals were synthesized using a chemical synthetic route reported in a previous work.[32,33] Multilayers of self-organized platinum NCs have been elaborated through a close control of the solvent evaporation process after the synthesis. A TEM copper grid coated with amorphous carbon is placed at the bottom of a glass vial (height 1 cm, width 0.3 cm). The vial is filled with 200 μL of a suspension of the nanoparticles stabilized in toluene, which is then slowly evaporated for around 12 h. Two parafilm sheets have been used to close the vial aperture in order to slow down the evaporation process, with the container being kept at constant room temperature. A low suspension concentration of 2×10^{-5} mol·L^{-1} has been used in order to limit the thickness of the multilayers.

Electron Tomography Experiments. Experimental data for tomography were acquired by means of a JEOL 2100F transmission electron microscope with a field emission gun operating at 200 kV. The acquisition software, plugged in the Digital Micrograph software, provides an automated acquisition of the tilt series by varying the tilt angle step-by-step and by controlling the defocusing and the specimen drift at each tilt angle. In addition, it allows the automatic adjustment of the focal point of the beam in order to ensure that the focus is maintained on the tilted specimen. The tilt series of TEM BF images were recorded with a 2048 $\times$ 2048 pixel cooled CCD detector having a pixel size of about 0.25 nm and a 1 s exposure time for each record. The angular interval sampled during the acquisition was between 70 and $-70°$, with a tilt increment given by a 2° Saxton scheme, giving a total of 90 images. Once the acquisition of the tilt series was completed, the images were first roughly aligned using a cross-correlation algorithm. A refinement of this initial alignment was then obtained with the IMOD software,[34] where 5 nm gold beads deposited on the membrane supporting the specimen were used as fiducial markers. The volume reconstructions were computed using algebraic reconstruction techniques (ART)[35] implemented in the TomoJ software[36] with a number of iterations not exceeding 20. Visualization and quantitative analysis of the final volumes were carried out using Slicer and ImageJ software.

Conflict of Interest: The authors declare no competing financial interest.

REFERENCES AND NOTES

1. Lin, M.-H.; Chen, H.-Y.; Gwo, S. Layer-by-Layer Assembly of Three-Dimensional Colloidal Supercrystals with Tunable Plasmonic Properties. *J. Am. Chem. Soc.* **2010**, *132*, 11259–11263.
2. Chen, W.; Chen, C.; Guo, L. Magnetization Reversal of Two-Dimensional Superlattices of Mn_3O_4 Nanocubes and Their Collective Dipolar Interaction Effects. *J. Appl. Phys.* **2010**, *108*, 043912(1−8).
3. Courty, A.; Mermet, A.; Albouy, P. A.; Duval, E.; Pileni, M. P. Vibrational Coherence of Self-Organized Silver Nanocrystals in FCC Supra-Crystals. *Nat. Mater.* **2005**, *4*, 395–4006.
4. Lisiecki, I.; Halté, V.; Petit, C.; Pileni, M.-P.; Bigot, J.-Y. Vibration Dynamics of Supra-Crystals of Cobalt Nanocrystals Studied with Femtosecond Laser Pulses. *Adv. Mater.* **2008**, *20*, 4176–4179.
5. Quinten, M.; Leitner, A.; Krenn, J. R.; Aussenegg, F. R. Electromagnetic Energy Transport *via* Linear Chains of Silver Nanoparticles. *Opt. Lett.* **1998**, *23*, 1331–1333.
6. Brongersma, M. L.; Hartman, J. W.; Atwater, H. A. Electromagnetic Energy Transfer and Switching in Nanoparticle Chain Arrays below the Diffraction Limit. *Phys. Rev. B* **2000**, *62*, R16356–R16359.
7. Maier, S. A.; Kik, P. G.; Atwater, H. A.; Meltzer, S.; Harel, E.; Koel, B. E.; Requicha, A. A. G. Local Detection of Electromagnetic Energy Transport Below the Diffraction Limit in Metal Nanoparticle Plasmon Waveguides. *Nat. Mater.* **2003**, *2*, 229–232.
8. Sau, T. K.; Rogach, A. L. Nonspherical Noble Metal Nanoparticles:Colloid-Chemical Synthesis and Morphology Control. *Adv. Mater.* **2010**, *22*, 1781–1804.
9. Bodnarchuk, M. I.; Kovalenko, M. V.; Heiss, W.; Talapin, D. V. Energetic and Entropic Contributions to Self-Assembly of Binary Nanocrystal Superlattices: Temperature as the Structure-Directing Factor. *J. Am. Chem. Soc.* **2010**, *132*, 11967–11977.

10. Quan, Z.; Fang, J. Superlattices with Non-spherical Building Blocks. *Nano Today* **2010**, *5*, 390–411.
11. Demortière, A.; Buathong, S.; Pichon, B. P.; Panissod, P.; Guillon, D.; Bégin-Colin, S.; Donnio, B. Nematic-like Organization of Magnetic Mesogen-Hybridized Nanoparticles. *Small* **2010**, *6*, 1341–1346.
12. Weyland, M.; Midgley, P. A. Electron Tomography. *Mater. Today* **2004**, *6*, 32–40.
13. de Jong, K. P.; van den Oetelaar, L. C. A.; Vogt, E. T. C.; Eijsbouts, S.; Koster, A. J.; Friedrich, H.; de Jongh, P. E. High-Resolution Electron Tomography Study of an Industrial Ni−Mo/γ-Al_2O_3 Hydrotreating Catalyst. *J. Phys. Chem. B* **2006**, *110*, 10209–10212.
14. Ersen, O.; Parmentier, J.; Solovyov, L. A.; Drillon, M.; Pham-Huu, C.; Werckmann, J.; Schultz, P. Direct Observation of Stacking Faults and Pore Connections in Ordered Cage-Type Mesoporous Silica FDU-12 by Electron Tomography. *J. Am. Chem. Soc.* **2008**, *130*, 16800–16806.
15. Thomas, P. J.; Midgley, P. A. An Introduction to Energy-Filtered Transmission Electron Microscopy. *Top. Catal.* **2002**, *21*, 109–138.
16. Florea, I.; Ersen, O.; Hirlimann, C.; Roiban, L.; Deneuve, A.; Houllé, M.; Janowska, I.; Nguyen, P.; Pham, C.; Pham-Huu, C. Analytical Electron Tomography Mapping of the SiC Pore Oxidation at the Nanoscale. *Nanoscale* **2010**, *2*, 2668–2678.
17. Aronova, M. A.; Kim, Y. C.; Harmon, R.; Sousa, A. A.; Zhang, G.; Leapman, R. D. Three-Dimensional Elemental Mapping of Phosphorus by Quantitative Electron Spectroscopic Tomography (QuEST). *J. Struct. Biol.* **2007**, *160*, 35–48.
18. Mobus, G.; Doole, R. C.; Inkson, B. J. Spectroscopic Electron Tomography. *Ultramicroscopy* **2003**, *96*, 433–451.
19. Midgley, P. A.; Weyland, M. 3D Electron Microscopy in the Physical Sciences: the Development of Z-Contrast and EFTEM Tomography. *Ultramicroscopy* **2003**, *96*, 413–431.
20. Nellist, P.; Pennycook, S. J. Incoherent Imaging Using Dynamically Scattered Coherent Electrons. *Ultramicroscopy* **1999**, *78*, 111–124.
21. Bals, S.; Batenburg, K. J.; Verbeeck, J.; Sijbers, J.; VanTendeloo, G. Quantitative Three-Dimensional Reconstruction of Catalyst Particles or Bamboo-like Carbon Nanotubes. *Nano Lett.* **2007**, *7*, 3669–3674.
22. Kübel, C.; Voigt, A.; Schoenmakers, R.; Otten, M.; Su, D.; Lee, T.-C.; Carlsson, A.; Bradley, J. Recent Advances in Electron Tomography: TEM and HAADF-STEM Tomography for Materials Science and Semiconductor Applications. *J. Microsc. Microanal.* **2005**, *11*, 378–400.
23. Ahrenkiel, S. P.; Yu, R.; Murphy, J. E.; Nedeljkovic, J. M.; Donohoe, B. S. Nanoparticle Shape and Configuration Analysis by Transmission Electron Tomography. *J. Microsc.* **2007**, *230*, 382–387.
24. Friedrich, H.; Gommes, C. J.; Overgaag, K.; Meeldijk, J. D.; Evers, W. H.; de Nijs, B.; Boneschanscher, M. P.; de Jongh, P. E.; Verkleij, A. J.; de Jong, K. P.; *et al.* Quantitative Structural Analysis of Binary Nanocrystal Superlattices by Electron Tomography. *Nano Lett.* **2009**, *9*, 2719–2724.
25. Zhang, J.; Luo, Z.; Quan, Z.; Wang, Y.; Kumbhar, A.; Smilgies, D.-M.; Fang, J. Low Packing Density Self-Assembled Superstructure of Octahedral Pt_3Ni Nanocrystals. *Nano Lett.* **2011**, *11*, 2912–2918.
26. Miszta, K.; de Graaf, J.; Bertoni, G.; Dorfs, D.; Brescia, R.; Marras, S.; Ceseracciu, L.; Cingolani, R.; van Roij, R.; Dijkstra, M.; *et al.* Hierarchical Self-Assembly of Suspended Branched Colloidal Nanocrystals into Superlattice Structures. *Nat. Mater.* **2011**, *10*, 872–876.
27. Sun, Z.; Luo, Z.; Fang, J. Assembling Nonspherical 2D Binary Nanoparticle Superlattices by Opposite Electrical Charges: The Role of Coulomb Forces. *ACS Nano* **2010**, *4*, 1821–1828.
28. Liu, J.; Wang, L.; Sun, X.; Zhu, X. Cerium Vanadate Nanorod Arrays from Ionic Chelator-Mediated Self-Assembly. *Angew. Chem., Int. Ed.* **2010**, *49*, 3492–3495.
29. Baranov, D.; Fiore, A.; van Huis, M.; Giannini, C.; Falqui, A.; Lafont, U.; Zandbergen, H.; Zanella, M.; Cingolani, R.; Manna, L. Assembly of Colloidal Semiconductor Nanorods in Solution by Depletion Attraction. *Nano Lett.* **2010**, *10*, 743–749.
30. Florea, I.; Demortière, A.; Petit, C.; Bulou, H.; Hirlimann, C.; Ersen, O. Electron Tomography and 3D Molecular Simulations of Platinum Nanocrystals. *J. Phys. Chem. C*, submitted.
31. http://www.mathcurve.com/polyedres/octaedre_tronque/octaedre_tronque.shtml.
32. Podsiadlo, P.; Krylova, G. V.; Demortiere, A.; Shevchenko, E. V. Multicomponent Periodic Nanoparticle Superlattices. *J. Nanopart. Res.* **2011**, *13*, 15–32.
33. Demortière, A.; Launois, P.; Goubet, N.; Albouy, P.-A.; Petit, C. Shape-Controlled Platinum Nanocubes and Their Assembly into Two-Dimensional and Three-Dimensional Superlattices. *J. Phys. Chem. B* **2008**, *112*, 14583–14592.
34. Mastronarde, D. N. Dual-Axis Tomography: An Approach with Alignment Methods that Preserve Resolution. *J. Struct. Biol.* **1997**, *120*, 343–352.
35. Gordon, R.; Bender, R.; Herman, G. T. Algebraic Reconstruction Techniques for Three Dimensional Electron Microscopy and X-ray Photography. *J. Theor. Biol.* **1970**, *24*, 471–481.
36. Messaoudii, C.; Boudier, T.; Sanchez Sorzano, C. O.; Marco, S. TomoJ: Tomography Software for Three-Dimensional Reconstruction in Transmission Electron Microscopy. *Bioinformatics* **2007**, *6*, 288 (1−9).